PCCP

# Primary photodissociation mechanisms of pyruvic acid on $S_1$: observation of methylhydroxycarbene and its chemical reaction in the gas phase


| | |
|---|---|
| Journal: | *Physical Chemistry Chemical Physics* |
| Manuscript ID | CP-ART-12-2020-006424.R1 |
| Article Type: | Paper |
| Date Submitted by the Author: | 02-Feb-2021 |
| Complete List of Authors: | Samanta, Bibek; Univ. of Southern California, Department of Chemistry<br>Fernando, Ravin; Univ. of Southern California, Department of Chemistry<br>Rösch, Daniel; Sandia National Laboratories<br>Reisler, Hanna; Univ. of Southern California, Department of Chemistry<br>Osborn, David; Sandia National Laboratories, |
| | |

# Primary photodissociation mechanisms of pyruvic acid on $S_1$: observation of methylhydroxycarbene and its chemical reaction in the gas phase

B. R. Samanta[1], R. Fernando[1], D. Rösch[2], H. Reisler[1]*, and D.L. Osborn[2]*

## Abstract

Pyruvic acid, a representative alpha-keto carboxylic acid, is one of the few organic molecules destroyed in the troposphere by solar radiation rather than by reactions with free radicals. To date, only its stable final products were identified, often with contribution from secondary chemistry, making it difficult to elucidate photodissociation mechanisms following excitation to the lowest singlet excited-state ($S_1$) and the role of the internal hydrogen bond in the most-stable Tc conformer. Using multiplexed photoionization mass spectrometry we report the first direct experimental evidence, via the observation of singlet methylhydroxycarbene (MHC) following 351 nm excitation, supporting the decarboxylation mechanism previously proposed. Decarboxylation to MHC + $CO_2$ represents 97 – 100% of product branching at 351 nm. We observe vinyl alcohol and acetaldehyde, which we attribute to isomerization of MHC. We also observe a 3 ± 2% yield of the Norrish Type I photoproducts $CH_3CO$ + DOCO, but only from $d_1$-pyruvic acid. At 4 Torr pressure, we measure a photodissociation quantum yield of $1.0^{+0}_{-0.4}$, consistent with IUPAC recommendations. However, our measured product branching fractions disagree with IUPAC. In light of previous calculations, these results support a mechanism in which hydrogen transfer on the $S_1$ excited state occurs at least partially by tunneling, in competition with intersystem crossing to the $T_1$ state. We present the first evidence of a bimolecular reaction of MHC in the gas phase, where MHC reacts with pyruvic acid to produce a $C_4H_8O_2$ product. This observation implies that some MHC produced from pyruvic acid in Earth's troposphere will be stabilized and participate in chemical reactions with $O_2$ and $H_2O$, and should be considered in atmospheric modeling.

## I. Introduction

The ultraviolet (UV) photodissociation of organic molecules and the dissociation dynamics that lead to final products are fundamental processes that govern reactions in the atmosphere, reactivity on the surface of organic aerosols, and biological damage caused by UV irradiation. The nature of the initially excited state, its coupling mechanism to other electronic states, and the kinetic competition between possible pathways determine final products. In both laboratory and practical environments, discovering primary photochemical pathways is complicated by secondary reactions with other atoms and molecules, and it is often challenging to correlate observed outcomes with primary photodissociation steps.

Pyruvic acid (PA, $CH_3COCOOH$), a representative of α-keto carboxylic acids, has multiple sources in Earth's atmosphere[1-8] including photo-oxidation of isoprene and direct emissions.[9, 10] Unlike most volatile organic compounds it reacts slowly with OH radicals,[11-13] so

that destruction by solar radiation is believed to be its main sink.[11, 12] The solar actinic flux near the Earth's surface overlaps with the lowest energy absorption band of PA (290-380 nm), which has a maximum around 350 nm.[14-17] Dissociation via this band, which accesses the $S_1$ excited state by a $\pi^* \leftarrow n$ transition, has attracted considerable research interest but also some controversy. The primary photoproducts are believed to be $CO_2$ and methylhydroxycarbene (MHC), although this carbene has never been observed in PA photodissociation, presumably because it rapidly isomerizes to its most stable isomer – acetaldehyde (Ac).[17-19] When PA's photodissociation is investigated in the presence of buffer gases such as $O_2$, $N_2$, air, and water in an atmospheric simulator, many other products, including acetic acid, $H_2CO$, $CH_4$, $CH_3OH$, and CO are also observed.[14, 15, 18, 20] These studies document relative product yields that depend in a complicated way on the partial pressure of PA and the pressure and nature of the buffer gas. Most of these experiments, however, were carried out in static gas cells where nascent products were subject to prolonged irradiation and secondary reactions.[14, 15, 17-20] Furthermore, one must be careful in interpreting the term "quantum yield" for photo-destruction of PA or photo-production of products, because some authors use this term to denote only the primary photodissociation events, whereas in other cases the authors include all secondary chemistry that is induced under prolonged irradiation and at all wavelengths covered by the solar actinic flux. Not surprisingly, these studies often disagree amongst one another on the mechanism, product yields, and the roles of the electronic ground and excited $S_1$ and $T_1$ states.

**Table 1:** Primary photodissociation pathways of PA and their heats of reaction evaluated at 0 K.

| Reaction | | $\Delta H^0_{rxn}$ (kcal mol$^{-1}$) | |
|---|---|---|---|
| $CH_3C(O)C(O)OH + h\nu \rightarrow$ | $CH_3COH + CO_2$ | $44.0 \pm 1.3$ | (R1) |
| | $H_2C{=}CHOH + CO_2$ | $3.6 \pm 0.6$ | (R2) |
| | $CH_3CHO + CO_2$ | $-6.5 \pm 0.6$ | (R3) |
| | $CH_3C(O)OH + CO$ | $-2.8 \pm 0.6$ | (R4) |
| | $CH_3CO + HOCO$ | $80.4 \pm 0.6$ | (R5) |

The primary photochemical processes considered in this study are summarized in Table 1. Thermochemical values used are at 0 K and taken from the Active Thermochemical Tables[21] unless otherwise noted. The electronic supplementary information (ESI) provides additional thermochemical sources.

A 2019 IUPAC datasheet[22] summarizes the current understanding of PA's photochemistry. The task group invokes product channels R3 – R5 and suggests wavelength-independent branching fractions of 0.6 (R3), 0.05 (R4), and 0.35 (R5) with a zero-pressure total photodissociation quantum yield of 1.0 that drops to $0.2 \pm 0.1$ in 1 bar air at 298K. The datasheet provides no guidance on yields of (R1) or (R2). Nevertheless, it acknowledges "divergence in experimental datasets and the poorly constrained role of secondary reactions." Therefore, despite significant effort, the most fundamental questions remain — what are PA's nascent photoproducts and what is the photodissociation mechanism? Rather than attempting to simulate the atmospheric photochemical environment, our goal in this study is to gain insight into the

primary steps of the dissociation mechanism by probing the photodissociation of PA highly diluted in an unreactive noble gas.

On the ground electronic state, $S_0$, PA has two low-lying conformers, Tc and Tt, as shown in Figure 1, with Tc (cis-keto) comprising 97% at ambient temperature.[20, 23-26] The lower energy conformer, Tc, is stabilized by a hydrogen bond (H-bond) between the acidic hydrogen and the oxygen of the ketonic group. Theoretical studies on the $S_1$ state of PA emphasize the importance of the H-bond on the dissociation dynamics.[27] Chang et al. calculated the height of the barrier to H-transfer from the carboxylic to the ketonic group on the $S_1$ potential energy surface (PES) of the Tc conformer of PA.[27] They propose an indirect decarboxylation mechanism that starts with H-transfer on $S_1$, followed by passage through a conical intersection to $S_0$ where decarboxylation takes place. Competing with this pathway, they also find rather efficient spin-orbit coupling to the close-lying $T_1$ triplet state, which may lead to the Norrish Type I reaction products typical in carbonyls — acetyl ($CH_3CO$) and hydroxyformyl (HOCO) radicals.

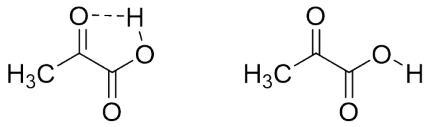


**Figure 1:** The cis- and trans-keto conformers of PA, Tc and Tt.

In our previous work we measured resonance-enhanced two-photon photofragment yield spectra of PA in a molecular beam, in which the $S_1 \leftarrow S_0$ transition was the one-photon resonant step. These spectra show that the $S_1$ state lives for a time longer than a vibrational (or even rotational) period, and that several low frequency skeletal modes are efficiently excited in the $S_1$ state.[28] For 351 nm excitation (81.5 kcal $mol^{-1}$), the excess energy available to products in the lowest-energy decarboxylation pathway (R1, forming $CO_2$ + MHC) is 37.5 kcal $mol^{-1}$, which is above the isomerization barriers connecting MHC to both the acetaldehyde and vinyl alcohol (VA) tautomers.[29, 30] The only $C_2H_4O$ isomer observed to date, following $S_1$ photodissociation of PA, was acetaldehyde.

In pyrolysis of PA on $S_0$, MHC was stabilized when captured in a cold Ar matrix,[30] but MHC formed in this way has little rovibrational energy, and thus its fate may not be the same as in PA photodissociation. In calculations carried out on the $S_0$ PES, Takahashi et al. found that complete H-transfer in the Tc-conformer can occur within 200 fs at energies near the dissociation threshold.[29] This time scale was based on a combination of measurements of the linewidth of OH overtones in the PA vibrational absorption spectrum and dynamical calculations on the $S_0$ PES. The calculations suggested that rapid H chattering followed by H transfer to the carbonyl group was the first step in the decarboxylation reaction on $S_0$.[29]

We report here the first direct observation of MHC following $S_1$ excitation of PA and, moreover, we show that it decays within less than a millisecond. It is highly likely that MHC

decays via tautomerization to its more stable isomers, acetaldehyde and vinyl alcohol, and we provide direct evidence that MHC is also consumed in a bimolecular chemical reaction. We obtain similar results with $CH_3COCOOD$ ($d_1$-PA) and observe that the lifetime of the deuterated MHC is slightly longer than the fully hydrogenated isotopologue. In addition, we directly observe the Norrish Type I bond fission products $CH_3CO$ and DOCO, providing indirect evidence of $d_1$-PA dissociation via the triplet $T_1$ PES. These findings, combined with insights from theoretical work, lead us to suggest a mechanism for the photodissociation initiated on $S_1$.

Creation of gas phase MHC was first reported by Wesdemiotis and McLafferty,[31] who used fragmentation patterns in neutralization-reionization mass spectrometry to make this assignment. Later, Schreiner unambiguously formed MHC in the gas phase from vacuum pyrolysis of pyruvic acid, trapping it in a cryogenic matrix where it was identified by infrared spectroscopy.[30] MHC is challenging to detect in the gas phase, likely due to its high reactivity and the difficulty of distinguishing it from its more stable tautomers. Because of their hypothesized participation in sugar formation in prebiotic environments, bimolecular reactions of hydroxycarbenes have been of particular interest.[32] Recently, Schreiner and coworkers showed that the reaction between hydroxycarbene (HCOH, trapped in an Ar matrix) and formaldehyde can form glycolaldehyde via a barrierless mechanism.[33] Here we show prima facie evidence of a condensation type reaction involving MHC with pyruvic acid.

## II. Materials and methods

PA (Sigma-Aldrich; 98%) is doubly distilled at 60 °C at <1 Torr vacuum to eliminate volatile impurities. Only the clear distillate is used, leaving behind a yellow crude liquid consisting mostly of photocatalyzed oligomers.[34, 35] A freshly distilled sample is used in each experiment. The multiplexed photoionization mass spectrometer (MPIMS) apparatus, developed by Osborn and coworkers, was employed in these experiments at the Chemical Dynamics Beamline at the Advanced Light Source (ALS) of Lawrence Berkeley National Laboratory. The MPIMS apparatus has been described in detail in previous publications.[36, 37] Helium flows (10 sccm) through a glass bulb containing PA maintained at 21°C (1 Torr vapor pressure) at 35 Torr total pressure. The PA/He sample flow is diluted with 240 sccm of pure He in the reactor tube (1.05 cm inner diameter, 62.5 cm length). Typical experimental flow conditions inside the reactor tube (4 Torr at 250 sccm flow) yield a total number density of □ $1.3\times10^{17}$ molecules $cm^{-3}$ and a PA number density of □ $1.5\times10^{14}$ molecules $cm^{-3}$.

Singly deuterated PA samples ($d_1$-PA, $CH_3COCOOD$) are prepared *in-situ* by combining a 20 sccm He flow through a glass bulb containing PA (21 °C; 36 Torr total with He) and a 10 sccm He flow through another glass bulb containing $D_2O$ (21 °C; 54 Torr total with He). Helium provides the balance of the total 250 sccm flow. This method yields ~97% pure $d_1$-PA, confirmed using a time-of-flight (TOF) mass spectrum obtained with the MPIMS apparatus.

351 nm radiation generated by a XeF excimer laser (10 Hz repetition rate) is used for photodissociation. Gas flow rates are sufficient to renew the gas mixture completely between

each laser pulse, thereby avoiding repeated irradiation of samples. Unfocused laser radiation (~ 35 mJ $cm^{-2}$) propagates along the length of the tube parallel to the gas flow direction. A polychlorotrifluroethylene 2300 wax (Halocarbon Products Corporation) coating on the quartz reactor tube suppresses loss of reactive species due to wall loss. The gas phase in the reactor tube is continuously sampled via a □650 μm diameter orifice in the reactor tube wall that forms a molecular beam, which is intersected by tunable, monochromatized vacuum ultraviolet (VUV) synchrotron radiation at the Chemical Dynamics Beamline. The cations produced by VUV ionization are analyzed with an orthogonal-acceleration TOF mass spectrometer coupled to a time-sensitive MCP-based detector. $Xe^+$ ions formed by autoionization (8s ← 5p) are used to calibrate the VUV photon energy. Mass calibration is achieved via a calibration gas mixture containing trace amounts of ethene, propene, and 1-butene. The MPIMS measures ion intensity as a function of m/z (mass resolution m/Δm = 1500), kinetic time (480 μs 10 – 90% measured risetime of a step-function input of NO photoproducts of the 351 nm photodissociation of $NO_2$, using a procedure described previously[38]), and VUV photon energy (typically 25 meV steps), providing time- and mass-resolved photoionization (PI) spectra of the neutral species present in the reactor tube. We also signal average at selected photon energies to obtain ion intensity as a function of m/z and kinetic time. The experimental PI spectra are normalized by the output of an SXUV-100 Photodiode (International Radiation Detectors, Inc.) to correct for changes in photon-flux as a function of VUV energy. Unless mentioned otherwise, the average pre-laser signal is subtracted from the time-resolved post-laser signal, so that negative signals represent species depleted as a result of the photodissociation laser, whereas positive signals represent species created as a result of the laser.

## III. Results and Discussion

### *1. Identification of photodissociation products*

We sample molecules continuously to record the time evolution of products formed in the photodissociation reaction. We identify molecular species using the TOF spectra obtained at selected VUV photon energies (see Figure 2). A TOF spectrum obtained at 10.25 eV shows that m/z = 44.03 is the most intense peak. At 14.1 eV, the most intense peak is at m/z = 44.00. Our mass calibration confirms the molecular formulas $C_2H_4O$ and $CO_2$, respectively, for these two peaks, and the kinetic time traces are typical of stable products. We detect three $C_2H_4O$ isomers: MHC, acetaldehyde, and vinyl alcohol, and confirm the identities of the latter two species by comparing their PI spectra to known spectra, as shown in Figure 3a. We further confirm $CO_2$ and $C_2H_4O$ as photoproducts by repeating the measurements with $d_1$-PA. At 10.25 eV we obtain the most intense peak at m/z = 45.03 ($C_2H_3DO$), whereas m/z = 44.00 remains the most intense peak at 14.1 eV. The dominant fragment ion formed from dissociative ionization of both PA and $d_1$-PA above 10.2 eV is m/z = 43.02 ($C_2H_3O^+$). Assuming dissociative ionization occurs by simple bond fission with no molecular rearrangement, the observation of the same fragment ion mass from both PA isotopologues indicates that the deuteration in $d_1$-PA is indeed achieved at the

acidic H site. We do not observe time-resolved signal from either CO or acetic acid ($CH_3C(O)OH$).

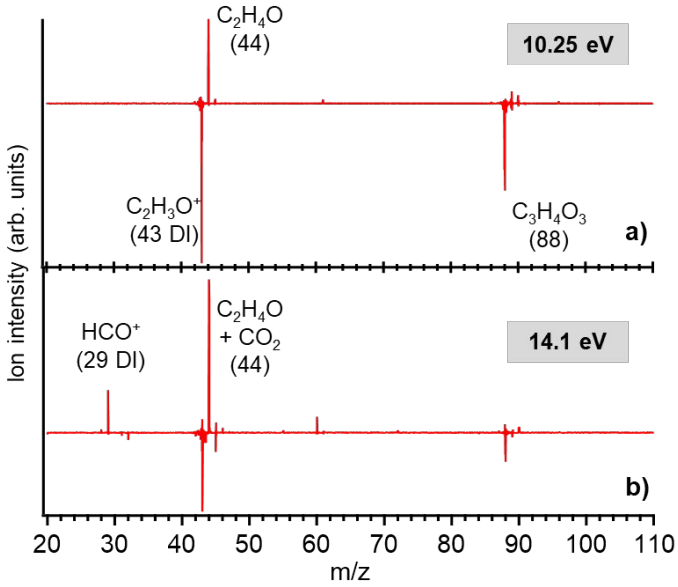


**Figure 2:** TOF spectra (integrated from 0 – 40 ms) of PA photodissociation at 351 nm obtained at (a) 10.25 eV and (b) 14.1 eV. The negative signals represent laser-depleted PA, observed at its parent mass and as fragment ions. $C_2H_4O$ isomers are identified in this study along with the co-product $CO_2$. $HCO^+$ is formed by dissociative ionization (DI) of $C_2H_4O$.

These results lead us to conclude that the primary photodissociation channel is decarboxylation of PA, yielding $C_2H_4O$ isomers as co-fragments of $CO_2$. Because the observed signal rise times are 480 μs, equal to the instrument response time, we rule out contributions of secondary reactions to these species. Products of secondary bimolecular reactions may be identified by signal rise times slower than the instrument response time. Referring to Figure 1, we propose that the nascent products of the 351 nm photodissociation of pyruvic acid following H-transfer from the carboxylic to the ketonic group are MHC and $CO_2$. It is likely that some of the MHC is formed with energy above its barriers to isomerization, and that this population of MHC rapidly interconverts with its more stable isomers in competition with cooling of all three $C_2H_4O$ isomers due to collisional energy transfer.

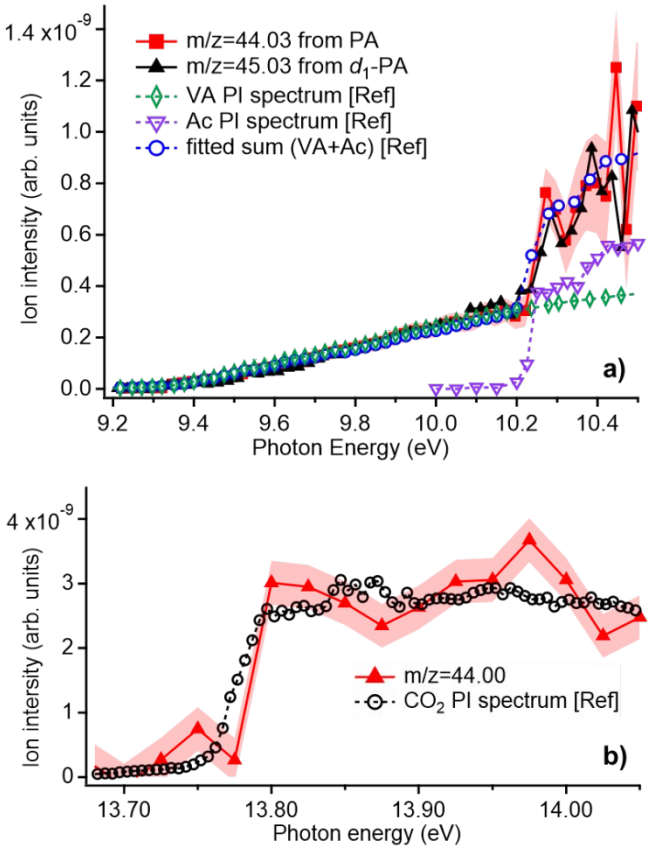


**Figure 3:** Photoionization (PI) spectra measured at (a) 9.2–10.5 eV showing the presence of both vinyl alcohol (VA) and acetaldehyde (Ac) photoproducts, and (b) 13.65–14.05 eV showing the $CO_2$ photoproduct. The photoproducts are identified by their exact m/z ratio and by comparing the PI spectra obtained in this work to reference PI spectra of these molecules.[38, 39] The shaded regions represent the error margins in the measured PI spectra of $C_2H_4O$ and $CO_2$ products (only the $d_0$-$C_2H_4O$ error is shown in the upper panel for clarity).

Whereas the time traces of m/z = 44.03 ($C_2H_4O$) above ~ 9.2 eV rise with an instrument limited risetime to a plateau, the shape of the time trace changes dramatically at photon energies below 9.1 eV, which is below the ionization energies (IEs) of both *syn*- and *anti*-vinyl alcohol of 9.30 and 9.17 eV, respectively.[40] Significant signal averaging (~ $1.2\times10^6$ laser shots) revealed a kinetic time trace with an instrument limited risetime but a fast decay, implying detection of an extremely reactive species at m/z = 44.03 for $d_0$-PA and m/z = 45.03 for $d_1$-PA, as shown in Figure 4(a). We could record the signal with acceptable signal-to-noise ratio (S/N) above 8.44 eV, and obtained the PI spectrum in Figure 4(b), which we assign to $d_1$-MHC. In a previous theoretical study, we estimated the adiabatic and vertical IEs of trans-MHC at 8.21 eV and 8.94 eV, respectively, with an uncertainty of 0.3 eV, consistent with the experimental spectrum of Figure 4(b).[41] Furthermore, the removal time is slightly slower for $d_1$-MHC (from $d_1$-PA) compared to $d_0$-MHC (from $d_0$-PA), as evident in the decay curves shown in Figure 4(a). We attribute this difference to slower isomerization or reactive loss of the deuterated isotopologue.

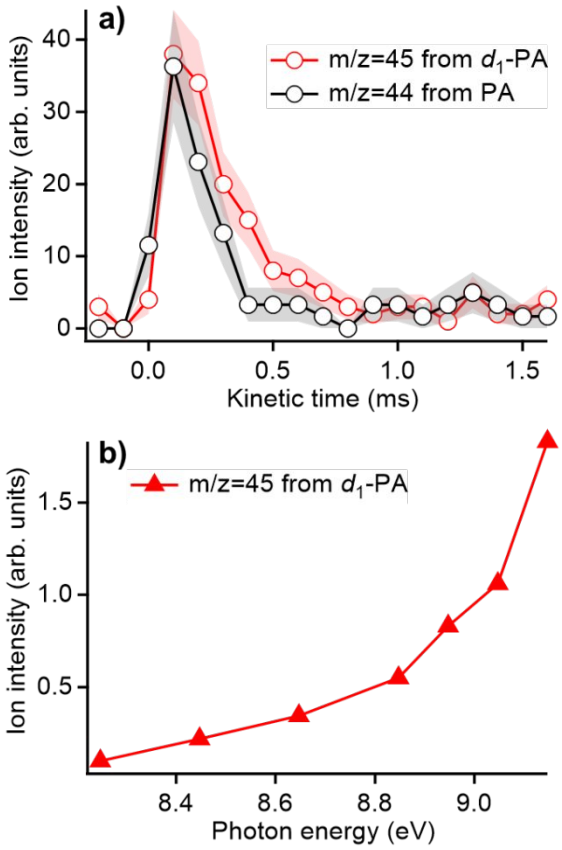


**Figure 4:** (a) Kinetic time traces of m/z = 44.03 (MHC) and m/z = 45.03 ($d_1$-MHC) from PA and $d_1$-PA photodissociation, respectively, integrated over 8.4 – 9.1 eV photon energies. The shaded regions represent the error bar at each data point. (b) The PI spectrum of m/z = 45.03 obtained in the photodissociation of $d_1$-PA.

Using the known absolute PI cross-sections of acetaldehyde and vinyl alcohol,[39] we determine that they are formed in the ratio of 2.1 ± 0.4 (favoring acetaldehyde) in the present experiments. This ratio is the same for both the $d_0$ and $d_1$ isotopologues of $C_2H_4O$. Previous studies in a cryogenic Ar matrix concluded that MHC products with low internal energy isomerize entirely to acetaldehyde, even though the isomerization barrier for this process is 6 kcal mol$^{-1}$ higher than that to vinyl alcohol.[30] This observation is consistent with isomerization via quantum mechanical tunneling because the barrier from MHC to acetaldehyde is narrower than the corresponding one to vinyl alcohol. This interpretation is reasonable in studies where the internal energy of MHC trapped in a cold Ar matrix is near the zero-point energy.[30] However, at higher temperatures (or higher internal energies), tunneling is expected to be less important. Given the low energetic threshold for decarboxylation of PA (R1; 44.0 kcal mol$^{-1}$) and the 351 nm photon energy of 81.5 kcal mol$^{-1}$, MHC can be formed with internal energies up to 37.5 kcal mol$^{-1}$ enabling isomerization to both acetaldehyde and vinyl alcohol products. Our observation of

significant isomerization of MHC to vinyl alcohol is evidence that tunneling is not the only isomerization mechanism of MHC in PA photodissociation at 300 K.

The nascent MHC photoproducts may have a broad distribution of internal energies from the dissociation dynamics. In the collisional environment of the reactor tube, MHC is expected to undergo ~20,000 collisions during the MPIMS instrument response time of ~ 0.5 ms. However, 99.9% of these collisions will be with He atoms, which will be less efficient for vibrational cooling compared to collisions with molecules. As a result, under the experimental conditions described in section II, we expect that many MHC molecules will have ample time to isomerize during vibrational thermalization. MHC isomerization to vinyl alcohol is calculated to have a barrier of 22.6 kcal $mol^{-1}$,[30] a lower barrier than that for isomerization to acetaldehyde (28 kcal $mol^{-1}$), and will be favored when MHC is produced with significant internal energy.[42] On the other hand, MHC products with less than ~ 22 kcal $mol^{-1}$ could only isomerize via tunneling. MHC has a measured tunneling half-life of ~ 1 hour when trapped in a 11 K Argon matrix in the absence of secondary reactions.[30] Although its tunneling lifetime when internally excited will be shorter than at 11 K, those MHC molecules with < 22 kcal $mol^{-1}$ internal energy may also decay via bimolecular chemical reactions, which we discuss in section III.3.

A previous experiment by Rosenfeld et al. at 351 nm, which reported detection of the $CO_2$ co-fragment, showed no infrared emission, and thus $CO_2$ was believed to be formed with little, if any, vibrational excitation.[43] Although collisional relaxation of the nascent $CO_2$ excitation in that experiment might have affected the observations, our results suggest that the internal energy in the MHC fragment is likely significant, based on the dominance of the more stable $C_2H_4O$ isomers we observe, though the fraction of the available energy disposed as product translational energy is unknown.

In a previous study we discovered a facile two-photon excitation of PA via $S_1$ (to $S_2$),[28] which at high laser fluence competed with one-photon dissociation. Therefore, we measured carefully the dependence of the yields of $C_2H_4O$ and $CO_2$ on laser fluence to confirm that in the present experiments, carried out at much lower laser fluence, they are formed by one-photon dissociation. We found that the product signals varied linearly with the 351 nm laser fluence (see ESI). In addition, the time trace of m/z = 88.02 (PA) showed depletion in signal of 0.33 ± 0.12 upon photodissociation at 30 mJ $cm^{-2}$. Our laser fluence ($7.2\times10^{16}$ photons $cm^{-2}$) combined with the reported absorption cross-section at 351 nm ($4.28\times10^{-20}$ $cm^2$)[16] predicts a percent absorption under our conditions of 0.31%. Within our experimental error of the measured fractional depletion of PA, we conclude that at 351 nm the primary quantum yield for photodissociation of PA is $\varphi_{diss}^{\mathrm{PA}} = 1.0\,^{+0}_{-0.4}$.

However, we also observe small but reproducible signals of m/z = 43 ($C_2H_3O$) and m/z = 46 ($DCO_2$) in $CH_3COCOOD$ ($d_1$-PA) photodissociation (see Figure 5) at photon energies as low as 8.8 eV. We assign these masses to the acetyl radical ($CH_3CO$; IE = 7.01 eV)[44] and the $d_1$-hydroxyformyl radical (DOCO; IE = 8.19 eV)[45], respectively, because no other species sharing

the same molecular formulae can be detected at such low photon energies. Fission of a C-C bond adjacent to the carbonyl group is common in dissociation of many carbonyls (knows as Norrish Type I reaction),[46] and has been seen in photodissociation of PA following excitation to $S_2$ and $S_3$.[28, 38] Although the Norrish Type I product channel (R5) in PA's $S_1 \leftarrow S_0$ photodissociation has been inferred in the literature,[14] to the best of knowledge it has never been directly observed. The dissociation energy of this channel (80.4 ± 0.6 kcal mol$^{-1}$ for $d_0$-PA) is only slightly below our excitation energy of 81.5 kcal mol$^{-1}$, which may contribute to the very low yield of this channel in the present experiments (see below). Note that we do not observe the corresponding product channel $CH_3CO$ + HOCO in the dissociation of $d_0$-PA.

Extrapolating the time traces in Figure 5 to time zero and utilizing the photoionization cross sections of $CH_3CO$, VA, and Ac, we extract a 0.06 ± 0.03 branching ratio of $CH_3CO$ : (Ac + VA). It is therefore clear that under our conditions, decarboxylation dominates over Norrish Type I fission. From the rest of our data and the absolute photoionization cross sections of $CO_2$ and PA, we extract the (Ac + VA) : $CO_2$ ratio of 0.5 ± 0.3. We utilize these values in a more comprehensive branching ratio analysis in section III.4.

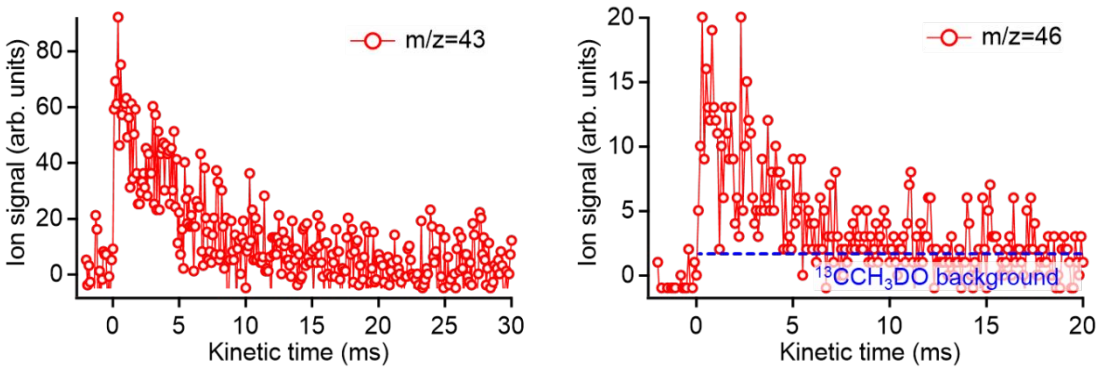


**Figure 5:** Kinetic time traces of $CH_3CO$ (left) and DOCO (right) from $d_1$-PA photodissociation at 9.65 eV IE. The $^{13}C$ background of the dominant $d_1$-vinyl alcohol product is shown by the blue dashed line on the right panel.

*2. Dissociation dynamics initiated on $S_1$*

A qualitative expectation of the dynamics when PA is excited to the $S_1$ state can be developed based upon the known molecular structure of the $S_0$ minimum and the nature of the $\pi^* \leftarrow n$ electronic excitation. Within the Condon approximation, photoexcitation to the $S_1$ state maintains the nuclear structure of the dominant Tc conformer (Figure 1) after the sudden promotion of a non-bonding electron on the keto oxygen to the $\pi^*$ orbital of the keto carbonyl. What was the O···H hydrogen bond in $S_0$ is now poised to develop a covalent interaction as the unpaired electron that remains in the non-bonding oxygen orbital interacts with the acidic hydrogen. Therefore, the electronic structure of the $S_1(n\pi^*)$ state should promote hydrogen transfer, while the pre-existing hydrogen bond provides the proper structural alignment for H transfer. However, based on the known photochemistry of the pure carbonyl molecules

acetaldehyde and acetone, it is also reasonable to expect intersystem crossing (ISC) from $S_1$ to a slightly lower-lying triplet surface ($T_1$), as shown in Figure 6. Once on the $T_1$ surface, Norrish Type I fission of a C-C bond adjacent to the keto group would be the expected outcome in a pure carbonyl molecule. In the case of pyruvic acid, the analogous pathway would produce either $CH_3CO$ + HOCO or $CH_3$ + COCOOH. However, the latter channel is calculated to be ~ 11 kcal $mol^{-1}$ endothermic for 351 nm excitation of PA, and therefore is not expected.[38]

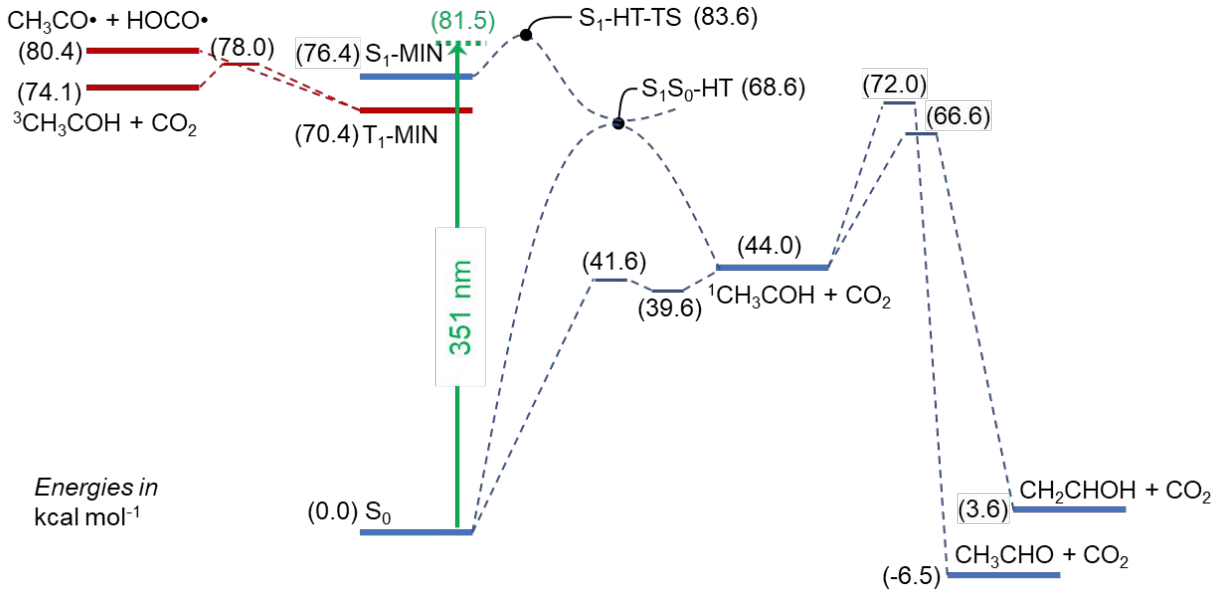


**Figure 6:** Stationary points on pyruvic acid potential energy surfaces. Singlet surfaces are shown in blue, the lowest triplet surface in red, and the 351 nm photon in green, with energies in kcal $mol^{-1}$. $S_1$-HT and $S_0$-HT are the hydrogen-transferred isomers of $S_1$ and $S_0$, respectively. The $S_1$-HT energy is very close to the conical intersection with $S_0$, $S_1S_0$-HT. The energy values are taken from references 27, 30, 47 and 48, unless modified as explained in the main text or the ESI.

Calculations attest to the complexity of the dynamics following excitation to $S_1$. Chang et al. carried out the most comprehensive theoretical study to date of the dissociation of PA initiated on $S_1$ using the multi-state complete active state approach.[27] We utilize their excited state energies, with appropriate shifts when more accurate thermochemical values are available, to construct the schematic potential energy diagram shown in Figure 6. For example, Chang et al.'s $S_1 \leftarrow S_0$ transition (83.6 kcal $mol^{-1}$) is higher than the experimentally known origin transition energy of 76.37 kcal $mol^{-1}$.[28] More recent calculations by da Silva using the G3X-K method place the corresponding $S_1$ and $T_1$ minima at 75 and 69 kcal $mol^{-1}$,[47] in much better agreement with experiment, and we therefore place the $T_1$ minimum 6 kcal $mol^{-1}$ below the $S_1$ minimum. Incorporating these corrections to Chang et al.'s calculations, Figure 6 is consistent with the heuristic arguments in the previous paragraph. Most importantly, they predict a double-well potential for $S_1$, with an $S_1$ minimum near the Franck-Condon point separated from the more stable hydrogen-transferred isomer, denoted $S_1$-HT, by a barrier at 83.6 kcal $mol^{-1}$. Note

that this barrier lies slightly higher than the energy of a 351 nm photon (81.5 kcal $mol^{-1}$). The lower-energy $T_1$ surface has a similar double-well shape.

Chang et al. find that the hydrogen-transferred isomer $S_1$-HT lies very close to a triple conical intersection with $S_0$ and $T_1$ that could facilitate both internal conversion and intersystem crossing from $S_1$. They propose an efficient transfer to $S_0$ via this conical intersection, after which decarboxylation takes place by two routes. Some of the flux forms MHC + $CO_2$ directly after passing through the conical intersection, while another pathway is a reverse hydrogen transfer to the original PA structure, which could then proceed to thermal decarboxylation on $S_0$ as discussed by Takahashi et al.[29] and da Silva[48]. These two pathways may result in different quantum state distributions in the products, with the direct component being nonstatistical and the indirect route leading to a more statistical distribution. Finally, Chang et al. also predict that the conical intersection could funnel population to the $T_1$ surface, from which the spin-allowed products are $^3$MHC + $^1CO_2$, with an asymptotic energy of ~74 kcal $mol^{-1}$ (MHC has a singlet ground state and a singlet-triplet gap of 30 kcal $mol^{-1}$).[41, 49]

Competing with H transfer on $S_1$, Chang et al. invoke a second pathway for ISC via strong spin-orbit interaction of $S_1$ with $T_1$ near the Franck-Condon region, which avoids the need for H transfer to access $T_1$.[27] In our previous experimental studies of supersonically cooled PA,[28] the linewidths of the vibronic bands close to the band origin indicate that the $S_1$ state is fairly long-lived (>1 ps). We hypothesize that the long lifetime of $S_1$ could make the $S_1/T_1$ ISC near the Franck-Condon point (analogous to the usual $S_1/T_1$ mixing in carbonyl compounds) competitive with excited state hydrogen transfer forming the $S_1$-HT isomer and subsequent transfer to $T_1$ and $S_0$, at least at energies close to or below the $S_1$ → S1-HT barrier.

Indeed, there exists some experimental evidence for the participation of $T_1$ in the photodissociation. Yamamoto and Back find that the light emission observed following 340-380 nm excitation to $S_1$ can be partially quenched by adding air, which is known to quench triplet states by interaction with $O_2$.[17] They propose that $T_1$ gives rise to phosphorescence. Once on $T_1$, PA can dissociate via spin-allowed channels to $^2CH_3CO$ + $^2$HOCO in addition to $^3$MHC + $^1CO_2$. Relative to the $T_1$ minimum, Chang et al. also calculate that the barrier height to the $CH_3CO$ + HOCO channel (6.1 kcal $mol^{-1}$) is lower than that of the $CO_2$ + $^3$MHC channel (two barriers of 8.7 kcal $mol^{-1}$ for H-transfer on $T_1$ and 7.7 kcal $mol^{-1}$ for decarboxylation).[27] Therefore, accessing $T_1$ via ISC from near the Franck-Condon point, rather than via the triple conical intersection, may enhance Norrish Type I decomposition to $CH_3CO$ + HOCO. Nevertheless, at 351 nm the $CH_3CO$ and HOCO product channel (R5) is only 1 kcal $mol^{-1}$ exothermic, which may limit the yield of this product channel.†

In fact, we observe the Norrish Type I reaction channel only with $CH_3COCOOD$. As Figure 6 shows, a 351 nm photon does not contain enough energy for PA to surmount the $S_1$-HT-TS barrier, and it is plausible that the dominant mechanism for H atom transfer is tunneling through this barrier. We would then expect less efficient tunneling of the carboxylic D atom

through the barrier in $d_1$-PA compared to $d_0$-PA. The consequently longer $S_1$ lifetime in $d_1$-PA could enhance the ISC pathway to $T_1$ near the Franck-Condon point. Therefore, the lack of $CH_3CO$ + HOCO product in $d_0$-PA supports the hypothesis that the H (or D) transfer from $S_1$ to $S_1$-HT through the barrier plays a pivotal role in the ensuing dynamics. Differences in zero point energy upon deuteration are unlikely to affect the Norrish Type I channel because the unbound degree of freedom at the transition state is the C-C bond, which is mostly independent of acidic hydrogen motion. However, zero point energy differences might lead to a kinetic isotope effect in passage through the S1-HT-TS, which would further suppress D- vs. H-atom tunneling. The dynamics on $S_1$, which involves several coupled surfaces and a conical intersection, is likely to depend on excitation wavelength. We suggest, therefore, that future experiments should include an exploration of the Norrish Type I product yield at wavelengths longer and shorter than 351 nm.

Our results confirm that decarboxylation is the major dissociation pathway for both $d_0$-PA and $d_1$-PA at 351 nm, but we extract a (Ac + VA):$CO_2$ ratio of only 0.5 ± 0.3. As stated in the IUPAC datasheet,[22] a $CH_3CHO$ to $CO_2$ product ratio less than unity (0.1 – 0.6, depending on conditions) has been observed by many researches, some of whom attributed it to undetected vinyl alcohol.[17] We have observed the vinyl alcohol directly and accounted for its contribution to total $C_2H_4O$. Instead, we propose that MHC and $CO_2$ are formed in a 1:1 ratio as a result of photodissociation. Although we do not have experimental evidence ruling out direct formation of Ac or VA in the primary photodissociation dynamics, da Silva's calculations[48] place the barriers to direct production of these $C_2H_4O$ isomers on $S_0$ to be 24 – 31 kcal $mol^{-1}$ higher than the pathway to MHC. We therefore propose that 0.5 ± 0.3 of the initial MHC isomerizes to Ac and VA, while the remaining 0.5 ± 0.3 of the initial MHC population is stabilized and consumed via secondary (bimolecular and possibly termolecular) reactions. In the next section we present the first evidence of participation of MHC in a bimolecular reaction.

*3. Evidence for secondary reaction of MHC*

In addition to the mass peak at m/z = 88.02, which is assigned to PA, we observe a laser-induced peak at m/z = 88.05 in the TOF spectra obtained at photon energies less than 9.95 eV (below the IE of PA). This time-resolved mass peak corresponds to the molecular formula $C_4H_8O_2$, i.e. double the mass of MHC, and is henceforth denoted M because its molecular structure remains unknown. It is slightly heavier than the parent mass of PA ($C_3H_4O_3$) and, furthermore, it is present only after the 351 nm laser pulse, as shown in Figure 7. We observe species M at photon energies as low as 7.7 eV.

Several molecular species can be assigned the molecular formula $C_4H_8O_2$. We tested acetoin ($CH_3C(O)CH(OH)CH_3$) as a candidate because it has been previously observed in photolysis of PA in aqueous solutions.[12, 50] However, our PI spectrum obtained from an authentic acetoin sample does not conclusively match the PI spectrum of species M (see ESI). We found that in photodissociation of $d_1$-PA, the M peak shifted to m/z = 90.06, as shown in Figure 8(a).

The double deuteration suggests that M is a result of a bimolecular reaction between two singly deuterated species.

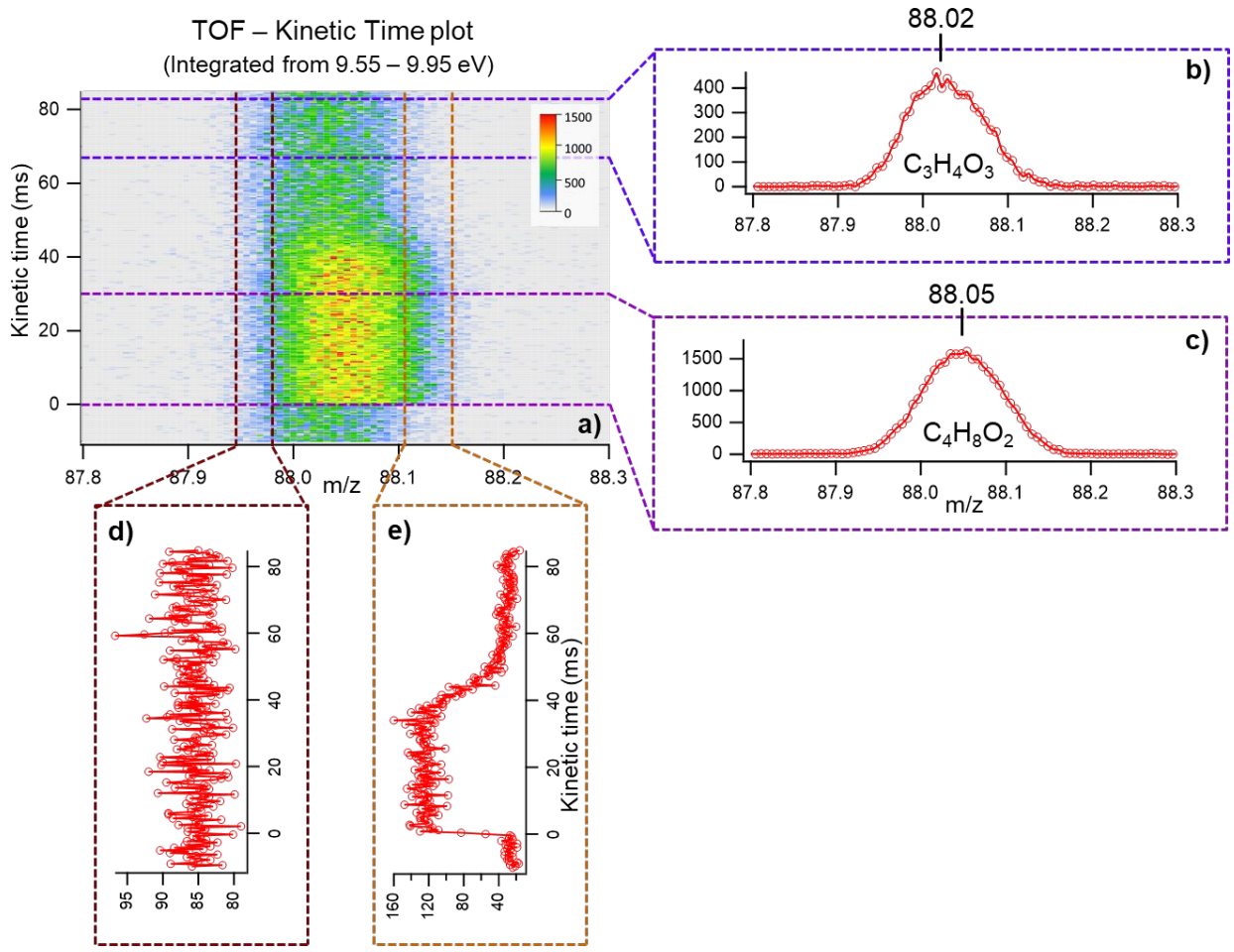


**Figure 7:** (a) Plot of ion signal vs. kinetic time and m/z in the vicinity of m/z = 88 (integrated from 9.55 – 9.95 eV). The pre-photodissociation background is not subtracted. Two distinct mass peaks are present after integration over kinetic time windows: (b) when all reaction products have been pumped out (65 – 84 ms) and (c) when photodissociation products are present in the tube (0 – 30 ms). (d) Kinetic time plot obtained by integration over the lighter mass. (e) Kinetic time plot of the heavier mass (species M) showing a time trace typical of a stable photoproduct.

Schreiner and coworkers have recently demonstrated the formation of glycoaldehyde ($CH_2(OH)CHO$) in an Ar matrix, and proposed a reaction between hydroxycarbene (HCOH) and formaldehyde ($H_2CO$) as a possible source.[33] However, a similar reaction between vibrationally excited MHC and one of the $C_2H_4O$ photoproducts is unlikely under our experimental conditions. Assuming a quantum yield of 1.0 for MHC from PA photodissociation, MHC can undergo a maximum of 0.15 collisions per millisecond with $C_2H_4O$ isomers (including another MHC). Thus, the possibility of product formation by recombination of two colliding $C_2H_4O$ molecules is ruled out because the rise time of species M in Figure 8(c) is much faster than the inverse of this collision rate (~7 ms).

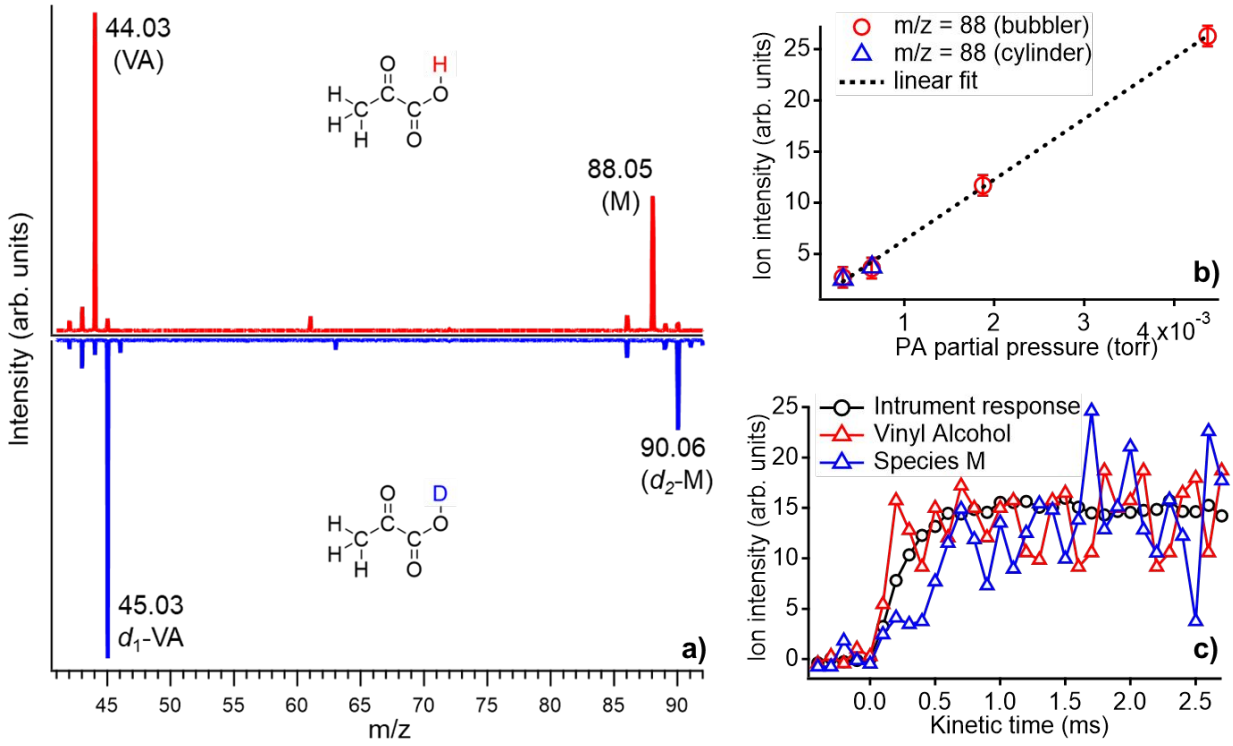


**Figure 8:** (a) TOF spectra (integrated over 5 – 40 ms) of PA (red trace) and $d_1$-PA (blue trace, inverted for clarity) showing the observed change in mass peaks due to deuteration. (b) Species M signal changes linearly upon change in PA concentration and is independent of the mode of PA sample preparation demonstrated by two different methods: (i) He bubbled through a glass bulb containing PA (red circles) and (ii) sample mixture delivered via a cylinder (blue triangles). (c) At low PA partial pressure (0.3 mTorr) species M shows a slower rise time, whereas VA, formed by rapid isomerization of vibrationally excited primary photoproduct MHC, shows a rise time limited by the instrument response time. The data in this figure are all obtained at a photon energy of 9.65 eV.

By contrast, the number of collisions between MHC and PA can be as high as 45 per millisecond under our experimental conditions. Furthermore, singlet carbenes are typically highly reactive (see section III.4 for further discussion).[51-55] Therefore, a collision between MHC and PA may result in decarboxylative condensation to create the covalently bonded species M. We tested this hypothesis by running a set of experiments as a function of PA concentration to measure the order of the reaction producing M. At higher partial pressures we used a bubbler to introduce PA into the reaction tube, as described in section II, whereas to reach lower partial pressures we diluted PA further in a gas cylinder. This approach allowed us to vary the concentration of PA by a factor of 10. We find that the signals of primary photoproducts such as vinyl alcohol, acetaldehyde, and $CO_2$ depend linearly on PA partial pressure, as expected. We also observed that the dependence of the signal of species M on PA concentration is linear. Because of the low absorption cross section of PA at 351 nm, the initial concentration of the MHC photoproduct is orders of magnitude smaller than the PA concentration. Thus, the MHC +

PA reaction would be pseudo-first order, consistent with the observed linear dependence of the signal of M on PA concentration.

Furthermore, as we lower PA concentration, the *rate* of the MHC + PA reaction should decrease, so that at sufficiently low PA concentration, the rise time of M would become longer than the instrument response time. Figure 8(c) shows such behavior, providing further evidence that M is indeed formed by a bimolecular reaction. To assess the kinetic feasibility of a bimolecular reaction between MHC and PA consider the following upper limit. Assuming a reaction rate coefficient, $k = 1x10^{-11}$ cm$^3$ molecules$^{-1}$ s$^{-1}$, approximately ten times lower than the maximum gas phase kinetic rate between two neutrals at 298 K, we obtain a first order reaction rise time of $t_{1/2} \approx 500$ μs for PA partial pressure of 5 mTorr, which is similar to the response time of the MPIMS instrument. This assumed (but reasonable) rate constant, would explain the fast removal time of MHC shown in Figure 4. Correspondingly, at the lowest partial pressure used in our experiments (~ 0.3 mTorr), where the signal of MHC itself is too weak to measure, the rise time of the M product should become longer than the response time, as seen in Figure 8(c), consistent with the bimolecular reaction hypothesis we propose. As discussed in section III.1, MHC photoproducts with less than 22 kcal mol$^{-1}$ internal energy will not isomerize to the more stable isomers and can react with PA.

Finally, we considered the possibility that mass M is a photodissociation product of PA dimers. A recent study by Vaida and coworkers showed that the Tt-Tt dimer of PA is relatively stable.[20] In this case, the M signal should have shown a quadratic dependence on PA pressure, which is inconsistent with the linear dependence observed in Figure 8(b). In addition, in dimer photodissociation, we do not expect an increase in the rise time at low PA pressures as seen in Figure 8(c). Furthermore, the low concentration of the Tt isomer (3%) at room temperature indicates that the gas phase results in the present work are dominated by the Tc isomer. We conclude that photodissociation of PA dimers is not the source of M.

In considering possible bimolecular reaction mechanisms, MHC and PA could form a pre-reactive H-bonded complex, which could enhance the rate constant for their bimolecular reaction. A condensation reaction ending in decarboxylation could be energetically feasible due to the nucleophilicity of MHC and the electrophilicity of the carbon centers on PA. Theoretical calculations of the mechanism of the reaction between PA and the MHC are needed to better understand the nature of the bimolecular reaction producing species M. However, our observation of only $d_2$-M from $d_1$-PA is strong evidence that when MHC attacks pyruvic acid, the reaction retains the acidic hydrogen of PA and removes one carbon and two oxygen atoms.

*4. Branching fractions and tropospheric implications*

Referring to reactions (R1) – (R5) from the introduction, we conclude that only (R1) and (R5) are primary product channels in the 351-nm photodissociation of PA, with (R1) dominating. From our data at 300 K and a total pressure of 4 Torr, we extract five quantities that can be used to calculate primary product branching fractions. They are:

$$\frac{[\mathrm{Ac}]}{[\mathrm{VA}]} = 2.1 \pm 0.4 \quad (1)$$

$d_1$-PA photodissociation, $$\frac{[\mathrm{CH_3CO}]}{[\mathrm{Ac + VA}]} = 0.06 \pm 0.03 \quad (2)$$

$d_0$-PA photodissociation, $$\frac{[\mathrm{CH_3CO}]}{[\mathrm{Ac + VA}]} = 0.00\,^{+0.03}_{-0.00} \quad (3)$$

$$\frac{[\mathrm{Ac + VA}]}{[\mathrm{CO_2}]} = 0.5 \pm 0.3 \quad (4)$$

$$\varphi^{\mathrm{PA}}_{diss} = 1.0\,^{+0}_{-0.4} \quad (5)$$

From these values we calculate primary branching fractions valid at 351 nm and 4 Torr:

$\mathrm{CH_3C(O)C(O)OD} + 351\ \mathrm{nm} \rightarrow \mathrm{CH_3COD^*} + \mathrm{CO_2}$ $0.97 \pm 0.02$ (R1)

$\mathrm{CH_3CO} + \mathrm{DOCO}$ $0.03 \pm 0.02$ (R5)

$\mathrm{CH_3C(O)C(O)OH} + 351\ \mathrm{nm} \rightarrow \mathrm{CH_3COH^*} + \mathrm{CO_2}$ $1.00\,^{+0}_{-0.02}$ (R1)

$\mathrm{CH_3CO} + \mathrm{HOCO}$ $0.00\,^{+0.02}_{-0}$ (R5)

where $CH_3COD^*$ denotes internally excited MHC that may undergo isomerization to VA and Ac in competition with collisional cooling to stabilized MHC, denoted $CH_3COD$. We cannot distinguish an isotopic difference in the fate of MHC*, which under our conditions is:

$\mathrm{CH_3COH^*} + \mathrm{He} \rightarrow \mathrm{CH_3CHO}$ $0.34 \pm 0.20$ (R6)

$\mathrm{H_2C{=}CHOH}$ $0.16 \pm 0.10$ (R7)

$\mathrm{CH_3COH}$ $0.5 \pm 0.3$ (R8)

Our 351 nm results agree with the IUPAC dissociation quantum yield of 1.0 at low pressure, but substantially disagree with IUPAC's chosen branching ratios of 0.6 ± 0.1 (R3), 0.05 ± 0.05 (R4), and 0.35 ± 0.1 (R5).[22] IUPAC provides no guidance on (R1), (R2), (R7), or (R8). It is not easy to divine a clear correspondence between the IUPAC-recommended, wavelength-independent branching ratios of (R3) – (R5) and the underlying primary data. Based on our understanding of the potential energy surfaces, it seems unlikely that additional product channels would become active at wavelengths longer than 351 nm, and the thermochemistry implies that (R5) will be of negligible importance for $\lambda > 351$ nm. We conclude that all other products observed in previous PA photodissociation studies arise either from secondary chemical reactions due to long irradiation times and the availability of reactive partners, or from excitation at wavelengths shorter than 351 nm. Additional wavelength-dependent studies of PA in noble gases would be valuable in this regard.

Next, we consider the effects this work may have on our understanding of PA photochemistry in the troposphere. Increasing pressure to 1 bar will increase the rate of collisional energy cooling of MHC*. Assuming that collisions with $N_2$ will be non-reactive, we anticipate that the main effect of increased pressure will be to increase stabilization to $CH_3COH$

(R8) at the expense of Ac and VA production. Two studies provide support for this conclusion. Heazlewood et al. observed extensive H/D scrambling when $CD_3CHO$ is excited with 87 – 91 kcal $mol^{-1}$ photons in a collisionless environment.[42] Master equation modeling in the collisionless limit revealed an average of 20 H- or D-shifts occurring before products are formed at the lower part of this energy range, in agreement with significant experimental production of DCO radicals. Crucially, the master equation could only reproduce experiment when the isomerization pathway included MHC. Furthermore, most of the flux followed the lowest energy pathway of Ac ↔ VA ↔ MHC ↔ VA ↔ Ac, rather than the higher barrier pathway connecting Ac directly to MHC. This study provides definitive evidence of efficient isomerization in $C_2H_4O$ at energies relevant to PA excited at 351 nm.

Later, Shaw et al. observed that photoexcitation of acetaldehyde with 87 – 95 kcal $mol^{-1}$ photons leads to phototautomerization and collisional stabilization of VA even at 1 bar pressure of $N_2$.[56] However, the extent of phototautomerization is pressure dependent. At 88 kcal $mol^{-1}$ photon energy, VA yield decreases from 24% near 0 bar to 6% at 1 bar. This reduction is consistent with our expectations of collisional energy cooling: at infinite pressure the rate of collisional cooling would exceed the rate of isomerization, and would produce only the initial isomer formed (acetaldehyde in the case of Shaw's experiments). As pressure decreases, the rate of collisional cooling decreases, enabling isomerization to distribute the population among different tautomers before stabilization locks in the populations. The excitation energy in these two studies provides the MHC isomer of $C_2H_4O$ with 36 to 44 kcal $mol^{-1}$ of energy, very similar to the maximum internal energy of ~ 38 kcal $mol^{-1}$ possible in MHC from PA photodissociation at 351 nm. Therefore, we expect that increased pressure will increase the fraction of MHC* that is stabilized to MHC when PA absorbs sunlight. Because of the dominant sequential MHC ↔ VA ↔ Ac pathway of $C_2H_4O$ isomerization observed by Heazlewood, it is possible that as the MHC stabilization increases with increasing pressure, VA would be reduced less than Ac, making the Ac:VA ratio also pressure dependent. Master equation calculations could predict these pressure-dependent dynamics, but are beyond the scope of this study. Nevertheless, this trend leads us to conclude that stabilized MHC, and its possible chemical reactions, will be more important at 1 bar than they are at 4 Torr.

Eger et al. recently observed PA over a boreal forest, finding gas phase mixing ratios up to 327 pptv.[10] Based on the recommended IUPAC photodissociation quantum yield (0.2 at 1 atm) and branching fractions, they conclude that pyruvic acid is an important source of acetaldehyde in boreal environments. Our branching fraction for Ac production (0.34 ± 0.20) is lower than the IUPAC Ac branching fraction of 0.60. However, the IUPAC quantum yield for dissociation of 0.2 may be a significant underestimate, because it is based on a wide variety of experiments with an equally broad range of quantum yields, many of which include ill-defined secondary chemistry. Indeed, many of the previous experiments show quantum yields for $CO_2$ that are significantly higher than for Ac, but even these results have ambiguity due to long irradiation times. Furthermore, it is highly likely that VA production from PA photodissociation remains active at 1 bar in Earth's atmosphere. Shaw et al. concluded that the OH + VA + $O_2$ reaction

results in the formation of formic acid, with the effects most important over remote oceans.[56] The effect of photolytic production of VA from PA doesn't appear to be considered in any of the atmospheric literature related to pyruvic acid.

In addition, Eger et al.[10] suggest that MHC may react with $O_2$, producing $CH_3CO + HO_2$, as previously suggested by Reed Harris et al.[14] If true, the additional $CH_3CO$ would react with $O_2$ and $NO_2$ to form peroxyacetyl nitrate, an important reservoir species for $NO_2$. Although the $MHC + O_2 \rightarrow CH_3CO + HO_2$ reaction is plausible, we are not aware of any experimental or theoretical evidence to support this hypothesis. Lacking information on the reactivity of MHC, it may be informative to consider the most-studied carbene in the gas phase, methylene. $^1CH_2$ is removed in collisions with saturated and unsaturated hydrocarbons, $H_2$, and $H_2O$ with rate coefficients exceeding $1\times10^{-10}$ cm$^3$ molecule$^{-1}$ s$^{-1}$ at 300K.[53-55, 57, 58] However, $^1CH_2$ is actually the first electronically excited state of methylene, and hence removal of $^1CH_2$ results from a combination of collision induced intersystem crossing and reactive loss. Douglas et al.[54] measured that reactive loss accounts for 70% or more of total loss at 300 K, depending on the hydrocarbon co-reactant. By contrast, the rate coefficient for $^1CH_2$ removal from collisions with $O_2$ is $5\times10^{-11}$ cm$^3$ molecule$^{-1}$ s$^{-1}$ at 300 K, but product studies have shown that in this case $^1CH_2$ loss is dominated by collision-induced ISC to $^3CH_2$, which then reacts more slowly with $O_2$ with a rate coefficient of $3.2\times10^{-12}$ cm$^3$ molecules$^{-1}$ s$^{-1}$.[53] The ground electronic state of MHC is a singlet. We therefore expect the rate coefficients for MHC + $H_2$, hydrocarbons, or $H_2O$ to be of the order of $1\times10^{-10}$ cm$^3$ molecules$^{-1}$ s$^{-1}$ based on this comparison to singlet methylene. The MHC rate coefficient for reaction with $O_2$ could be as small as $10^{-12}$ but is likely larger. At a pressure of 1 bar, stabilization of recombination and addition reaction products will also be possible.

As pointed out by others, increasing the pressure may also cause vibrational relaxation on $S_1$.[17] Yamamoto and Back show that light emission is important at wavelengths from the $S_0$-$S_1$ band origin at 374 nm to ~345 nm, and is composed of fluorescence and phosphorescence. The former is not quenched at 350 nm even at air pressures > 100 Torr.[17] Increasing pressure from 4 Torr to 1 bar may therefore increase the importance of tunneling on $S_1$ from the Franck-Condon region to the hydrogen-transferred isomer. A longer lifetime of $S_1$ would also enhance ISC in the Franck Condon region. Vibrational relaxation on $S_1$ will become less important at wavelengths shorter than 350 nm, where light emission is greatly diminished.

## IV. Summary and Conclusions

Our experiments show that the total primary photodissociation quantum yield of pyruvic acid (PA) following $S_1 \leftarrow S_0$ excitation at 351 nm is $1.0 \pm 0.3$. The dominant product channel produces methylhydroxycarbene (MHC) and carbon dioxide (97% or more), with minor products acetyl + hydroxyformyl radicals (3% or less). The hydrogen bond in the Tc conformer of $S_0$ PA aligns the backbone of the molecule optimally for hydrogen transfer. The unpaired electron in the lone pair of the $S_1$ ($n\pi^*$) state provides the electronic driving force for hydrogen transfer on $S_1$. Following photoexcitation, our results support Chang et al.'s mechanism of an initial

dynamical competition between hydrogen transfer on $S_1$ and intersystem crossing from the Franck-Condon region to $T_1$. Offsetting the stationary points of the $S_1$ potential energy surface from Chang et al.'s calculations by the known experimental origin $S_1 \leftarrow S_0$ transition leads us to conclude that 351 nm excitation places PA slightly below the barrier for hydrogen transfer on $S_1$. Our observation of the Norrish Type I products $CH_3CO$ + DOCO from $d_1$-PA, but not $CH_3CO$ + HOCO from $d_0$-PA supports the hypothesis that H transfer, at least at 351 nm, occurs partially via tunneling. The heavier D atom should tunnel more slowly through the barrier to hydrogen transfer, allowing more time for intersystem crossing to compete, promoting the Norrish Type I products. The exponential dependence of tunneling rate on potential energy suggests that studies with longer and shorter wavelengths would be a sensitive test of the proposed mechanism. Additional theoretical studies are also needed to address the question of whether PA can also fragment on the $S_1$ surface itself, or whether, as in ketones and aldehydes, transfer to $T_1$ and $S_0$ is required before dissociation.

In previous studies of PA photodissociation in the actinic region relevant to Earth's troposphere, acetaldehyde was the only isomer of $C_2H_4O$ observed experimentally. Multiplexed photoionization mass spectrometry allowed us to directly observe both vinyl alcohol and methylhydroxycarbene as additional $C_2H_4O$ isomers. We propose that VA and Ac are not formed directly, but arise from the isomerization of the MHC that is formed with internal energy in excess of its barriers to isomerization. MHC isomerization to VA and Ac occurs by large amplitude hydrogen atom motion. The longer observed lifetime of $d_1$-MHC compared to $d_0$-MHC is consistent with the expected kinetic isotope effect for MHC's isomerization to VA and Ac, supporting our proposed mechanism.

These experiments provide a direct observation of MHC in the gas phase, and also the first observation of a bimolecular reaction of MHC. The only bimolecular reaction consistent with our kinetic data is the MHC + PA reaction, forming a $C_4H_8O$ product whose structure we cannot yet assign. The observation of the bimolecular reaction is evidence that a portion of the MHC formed in PA photodissociation has internal energies below its lowest barrier to isomerization. Therefore, one should expect the presence of MHC in the troposphere from photolysis of PA by sunlight, and the fraction of stabilized MHC is likely to increase at 1 bar compared our low-pressure conditions. The effect of vinyl alcohol production from PA photodissociation should also be included in atmospheric models, and may provide a source of additional formic acid. In the troposphere, MHC is unlikely to react with PA because it will collide first with other molecules (notably $N_2$, $O_2$, and $H_2O$) present in much higher concentrations. The products of these reactions are as yet unknown, but the rate coefficients are likely to be large ($10^{-12}$ cm$^3$ molecule$^{-1}$ s$^{-1}$ or larger). PA and related keto-acids could provide methods to create alkylhydroxycarbenes in the laboratory, enabling exploration of their reaction kinetics and reaction products that may in turn inform chemical models of complex reaction systems.

## V. Conflicts of interest

There are no conflicts to declare.

## VI. Acknowledgement

This research used resources of the Advanced Light Source, which is a DOE Office of Science User Facility under contract no. DE-ACO2-05CH11231. Support by the U.S. Department of Energy, Basic Energy Sciences, Grant No. DE-FG02-05ER15629 (HR) is gratefully acknowledged. This material is based upon work supported by the Division of Chemical Sciences, Geosciences and Biosciences, Office of Basic Energy Sciences (BES), US Department of Energy (USDOE). Sandia National Laboratories is a multimission laboratory managed and operated by National Technology and Engineering Solutions of Sandia, LLC, a wholly owned subsidiary of Honeywell International, Inc., for the USDOE's National Nuclear Security Administration under contract DE-NA0003525. This paper describes objective technical results and analysis. Any subjective views or opinions that might be expressed in the paper do not necessarily represent the views of the USDOE or the US Government.

## VII. Notes and References:

[1] Department of Chemistry, University of Southern California, Los Angeles, CA 90089-0482, United States
[2] Combustion Research Facility, Sandia National Laboratories, Livermore, California, 94551-0969, United States

[†] Our corrections to the potential energy diagram imply the $T_1$ barrier to $CH_3CO$ + HOCO is submerged below the energy of the separated products, which is likely incorrect. Additional excited state electronic structure calculations would be valuable to clarify the energetics.

Electronic supplementary information (ESI) available: Summary of fluence dependence of PA photoproducts at 351 nm, Photoionization spectrum of mass M, and reaction thermochemistry.

1. A. G. Carlton, B. J. Turpin, H. J. Lim, K. E. Altieri and S. Seitzinger, *Geophys. Res. Lett.*, 2006, L06822; DOI:10.1029/02005GL025374
2. A. Carlton, C. Wiedinmyer and J. Kroll, *Atmos. Chem. Phys.*, 2009, **9**, 4987-5005.
3. K. Kawamura, E. Tachibana, K. Okuzawa, S. Aggarwal, Y. Kanaya and Z. Wang, *Atmos. Chem. Phys.*, 2013, **13**, 8285-8302.
4. K. Ho, S. Lee, J. Cao, K. Kawamura, T. Watanabe, Y. Cheng and J. C. Chow, *Atmos. Environ.*, 2006, **40**, 3030-3040.
5. D. Grosjean, E. L. Williams and E. Grosjean, *Environ. Sci. Technol.*, 1993, **27**, 830-840.
6. M. O. Andreae, R. W. Talbot and S. M. Li, *J. Geophys. Res. Atmos.*, 1987, **92**, 6635-6641.
7. R. W. Talbot, B. W. Mosher, B. G. Heikes, D. J. Jacob, J. W. Munger, B. C. Daube, W. C. Keene, J. R. Maben and R. S. Artz, *J. Geophys. Res. Atmos.*, 1995, **100**, 9335-9343.

8. T. B. Nguyen, A. P. Bateman, D. L. Bones, S. A. Nizkorodov, J. Laskin and A. Laskin, *Atmos. Environ.*, 2010, **44**, 1032-1042.
9. K. J. Jardine, E. D. Sommer, S. R. Saleska, T. E. Huxman, P. C. Harley and L. Abrell, *Environ. Sci. Technol.*, 2010, **44**, 2454-2460.
10. P. G. Eger, J. Schuladen, N. Sobanski, H. Fischer, E. Karu, J. Williams, M. Riva, Q. Zha, M. Ehn, L. L. J. Quéléver, S. Schallhart, J. Lelieveld and J. N. Crowley, *Atmos. Chem. Phys.*, 2020, **20**, 3697–3711.
11. A. Mellouki and Y. Mu, *J. Photochem. Photobiol. A: Chem.*, 2003, **157**, 295-300.
12. E. C. Griffith, B. K. Carpenter, R. K. Shoemaker and V. Vaida, *Proc. Nat. Acad. Sci.*, 2013, **110**, 11714-11719.
13. J. R. Church, V. Vaida and R. T. Skodje, *J. Phys. Chem. A*, 2020, **124**, 790-800.
14. A. E. Reed Harris, M. Cazaunau, A. Gratien, E. Pangui, J.-F. Doussin and V. Vaida, *J. Phys. Chem. A*, 2017, **121**, 8348-8358.
15. A. E. Reed Harris, J.-F. Doussin, B. K. Carpenter and V. Vaida, *J. Phys. Chem. A*, 2016, **120**, 10123-10133.
16. A. Horowitz, R. Meller and G. K. Moortgat, *J. Photochem. Photobiol. A: Chem.*, 2001, **146**, 19-27.
17. S. Yamamoto and R. Back, *Can. J. Chem.*, 1985, **63**, 549-554.
18. M. G. Berges and P. Warneck, *Ber. Bunsenges. Phys. Chem.*, 1992, **96**, 413-416.
19. G. F. Vesley and P. A. Leermakers, *J. Phys. Chem.*, 1964, **68**, 2364-2366.
20. S. L. Blair, A. E. Reed Harris, B. N. Frandsen, H. G. Kjaergaard, E. Pangui, M. Cazaunau, J.-F. Doussin and V. Vaida, *J. Phys. Chem. A*, 2020, **124**, 1240-1252.
21. B. Ruscic and D. Bross, Active Thermochemical Tables (ATcT) values based on ver. 1.122p of the Thermochemical, ATcT.anl.gov, (accessed January, 2020).
22. IUPAC Task Group on Atmospheric Chemical Kinetic Data Evaluation, http://iupac.pole-ether.fr, (accessed January, 2021).
23. I. Reva, C. M. Nunes, M. Biczysko and R. Fausto, *J. Phys. Chem. A*, 2015, **119**, 2614-2627.
24. I. D. Reva, S. G. Stepanian, L. Adamowicz and R. Fausto, *J. Phys. Chem. A*, 2001, **105**, 4773-4780.
25. G. Buemi, *J. Phys. Org. Chem.*, 2009, **22**, 933-947.
26. V. Barone, M. Biczysko, J. Bloino, P. Cimino, E. Penocchio and C. Puzzarini, *J. Chem. Theory Comput.*, 2015, **11**, 4342-4363.
27. X.-P. Chang, Q. Fang and G. Cui, *J. Chem. Phys.*, 2014, **141**, 154311; DOI: 10.1063/1.4898085.
28. S. Sutradhar, B. R. Samanta, R. Fernando and H. Reisler, *J. Phys. Chem. A*, 2019, **123**, 5906-5917.
29. K. Takahashi, K. L. Plath, R. T. Skodje and V. Vaida, *J. Phys. Chem. A*, 2008, **112**, 7321-7331.

30. P. R. Schreiner, H. P. Reisenauer, D. Ley, D. Gerbig, C.-H. Wu and W. D. Allen, *Science*, 2011, **332**, 1300-1303.
31. C. Wesdemiotis and F. W. McLafferty, *J. Am. Chem. Soc.*, 1987, **109**, 4760-4761.
32. E. C. C. Baly, I. M. Heilbron and W. F. Barker, *J. Chem. Soc. Trans.*, 1921, **119**, 1025-1035.
33. A. K. Eckhardt, M. M. Linden, R. C. Wende, B. Bernhardt and P. R. Schreiner, *Nat. Chem.*, 2018, **10**, 1141-1147.
34. R. J. Perkins, R. K. Shoemaker, B. K. Carpenter and V. Vaida, *J. Phys. Chem. A*, 2016, **120**, 10096-10107.
35. R. J. Rapf, R. J. Perkins, B. K. Carpenter and V. Vaida, *J. Phys. Chem. A*, 2017, **121**, 4272-4282.
36. D. L. Osborn, P. Zou, H. Johnsen, C. C. Hayden, C. A. Taatjes, V. D. Knyazev, S. W. North, D. S. Peterka, M. Ahmed and S. R. Leone, *Rev. Sci. Instrum.*, 2008, **79**, 104103; DOI: 10.1063/1.3000004.
37. C. A. Taatjes, N. Hansen, D. L. Osborn, K. Kohse-Höinghaus, T. A. Cool and P. R. Westmoreland, *Phys. Chem. Chem. Phys.*, 2008, **10**, 20-34.
38. B. R. Samanta, R. Fernando, D. Rösch, H. Reisler and D. L. Osborn, *J. Chem. Phys.*, 2020, **153**, 074307; DOI: 10.1063/5.0018582.
39. T. A. Cool, K. Nakajima, T. A. Mostefaoui, F. Qi, A. McIlroy, P. R. Westmoreland, M. E. Law, L. Poisson, D. S. Peterka and M. Ahmed, *J. Chem. Phys.*, 2003, **119**, 8356-8365.
40. G. Y. Matti, O. I. Osman, J. E. Upham, R. J. Suffolk and H. W. Kroto, *J. Electron. Spectrosc. Relat. Phenom.*, 1989, **49**, 195-201.
41. B. R. Samanta, S. Sutradhar, R. Fernando, A. I. Krylov and H. Reisler, *J. Phys. Chem. A*, 2018, **122**, 6176-6182.
42. B. R. Heazlewood, A. T. Maccarone, D. U. Andrews, D. L. Osborn, L. B. Harding, S. J. Klippenstein, M. J. Jordan and S. H. Kable, *Nat. Chem.*, 2011, **3**, 443.
43. R. N. Rosenfeld and B. Weiner, *J. Am. Chem. Soc.*, 1983, **105**, 3485-3488.
44. R.-H. Li, J.-C. Wu, J.-L. Chang and Y.-T. Chen, *Chem. Phys.*, 2001, **274**, 275-281.
45. B. Ruscic and M. Litorja, *Chem. Phys. Lett.*, 2000, **316**, 45-50.
46. R. Norrish and C. Bamford, *Natur*, 1937, **140**, 195-196.
47. G. da Silva, personal communication.
48. G. da Silva, *J. Phys. Chem. A*, 2016, **120**, 276-283.
49. M. H. Matus, M. T. Nguyen and D. A. Dixon, *J. Phys. Chem. A*, 2006, **110**, 8864-8871.
50. P. A. Leermakers and G. F. Vesley, *J. Am. Chem. Soc.*, 1963, **85**, 3776-3779.
51. D. Polino, S. J. Klippenstein, L. B. Harding and Y. Georgievskii, *J. Phys. Chem. A*, 2013, **117**, 12677-12692.
52. W. Kirmse, *Carbene chemistry*, Elsevier, 2013.
53. M. A. Blitz, K. W. McKee, M. J. Pilling and P. W. Seakins, *Chem. Phys. Lett.*, 2003, **372**, 295-299.

54. K. M. Douglas, M. A. Blitz, W. Feng, D. E. Heard, J. M. Plane, H. Rashid and P. W. Seakins, *Icarus*, 2019, **321**, 752-766.
55. A. W. Jasper, S. J. Klippenstein, L. B. Harding and B. Ruscic, *J. Phys. Chem. A*, 2007, **111**, 3932-3950.
56. M. F. Shaw, B. Sztáray, L. K. Whalley, D. E. Heard, D. B. Millet, M. J. Jordan, D. L. Osborn and S. H. Kable, *Nat. Commun.*, 2018, **9**, 1-7.
57. W. Hack, H. G. Wagner and A. Wilms, *Ber. Bunsenges. Phys. Chem.*, 1988, **92**, 620-627.
58. G. J. Gutsche, W. D. Lawrance, W. S. Staker and K. D. King, *J. Phys. Chem.*, 1995, **99**, 11867-11874.